Journal of The Electrochemical Society, **152** (10) A2058-A2062 (2005)
0013-4651/2005/152(10)/A2058/5/$7.00 © The Electrochemical Society, Inc.

Modification of Sputter-Deposited Nanocrystalline $Li_xMn_{2-y}O_4$ Thin-Film Cathodes by In Situ Substrate Bias and Postanneal

K.-F. Chiu,[a,*,z] H. C. Lin,[b] K. M. Lin,[a] and C. H. Tsai

[a]*Department of Materials Science and Engineering, Feng Chia University, Taichung, Taiwan*
[b]*Department of Materials Science and Engineering, National Taiwan University, Taipei, Taiwan*

Thin films of lithium manganese oxides were deposited by radio frequency magnetron sputtering. Negative electric bias was applied on the substrates during deposition. The deposited films exhibited a defected spinel structure, $Li_xMn_{2-y}O_4$, as characterized by X-ray diffraction and micro-Raman spectroscopy. As the substrate bias increased, the films developed stronger (111) orientation. At high substrate bias, the films tended to lose lithium and a second phase of manganese oxide developed. Postanneal was also carried out to fabricate well-crystallized $LiMn_2O_4$ spinel thin films for comparison. The film morphology also varied with substrate bias as observed by scanning electron microscope. By substrate bias and anneal, well-crystallized films with different morphologies can be obtained. Charge–discharge and cyclic voltammetry curves of these thin films were measured and compared. The different electrochemical characteristics of these films were attributed to the modified crystallography, morphology, and film stress. The films deposited with in situ substrate bias exhibited larger capacity without well-defined plateau. The postannealed films without substrate bias showed well-defined 4.1 and 3.9 V plateaus with slightly lower capacity. The biased and annealed films had low capacity but showed only 3.5% of capacity loss after 30 cycles.
 [DOI: 10.1149/1.2034524]

Manuscript submitted January 26, 2005; revised manuscript received June 8, 2005. Available electronically August 25, 2005.

As the sizes of portable microelectronic devices rapidly decrease, microbatteries with lightweight high power density have become highly demanded. Thin-film electrodes with thickness of a few hundreds of nanometers or a few micrometers are therefore of great interest, especially for use in low-power applications, such as microelectronic and microelectromechanical systems.[1-4] For the thin-film cathodes, many different material systems have been considered and proved to be feasible. So far, lithium transition metal oxides are most popular and have been intensively studied in the last decade due to the rapid development of lithium-ion batteries.[1-10] Among them, $LiMn_2O_4$ is known as an economic and clean option.[11,12]

The structure of $LiMn_2O_4$ cubic spinel is composed of three-dimensional frameworks of Mn_2O_4, which provides interstitial space for lithium-ion intercalation and deintercalation. The chemical compositions can vary from $LiMn_2O_4$ to $Li_4Mn_5O_{12}$ with the spinel structure retained. It is referred to as the defected spinels[13,14] and the chemical formula can therefore be expressed as $Li_xMn_{2-y}O_4$, especially when it is in thin-film form, where the stoichiometry changes with process parameters. $Li_xMn_{2-y}O_4$ thin films prepared by physical vapor deposition exhibited nanocrystalline features, and post or in situ anneal can improve the crystallinity.[4,15-17]

The goal of this research is to study the influences of in situ bias on the sputtered deposited $Li_xMn_{2-y}O_4$thin thin films. Postannealing is also carried out for comparison. It is demonstrated that in situ substrate bias can effectively modify the film properties under a relatively low temperature ($>80°C$).

Experimental

The $Li_xMn_{2-y}O_4$ thin films were deposited on Si(100) wafers or stainless steel foils by radio frequency (rf) magnetron sputter deposition in a water-cooled vacuum chamber (base pressure $\sim 10^{-6}$ mbar). The target power density was kept at 5 W cm^{-2}, and the target/substrate distance was 70 mm. The $LiMn_2O_4$ sputtering target (2 in. diam) was made by solid-state reaction with the lithium content slightly higher than the ideal stoichiometry to ensure good sintered strength. The sintered target had a Li:Mn ratio of 1.29:2. The substrate holder was insulated from the chamber wall and biased negatively by a dc power supply. A thermocouple was embedded on it to monitor the depositing temperature, which was $<80°C$ after more than 2 h of deposition. The films were deposited with different in situ substrate biases. The sputtering gas was 99.9% pure Ar, and the working pressures were 2 Pa with a gas flow of 10 sccm. The typical deposition rate of these oxide thin films was around 7–8 nm/min. All of the films investigated were controlled at $\sim$500 nm thick by adjusting the deposition time.

The crystallography of the films deposited under different substte bias were characterized using Cu Kα X-ray diffraction (XRD). Micro-Raman spectroscopy (RS) was used to observe the local crystal structure evolution. The chemical composition of Li and Mn was measured by inductively coupled plasma atomic emission spectroscopy (ICP-AES, from Jarrel-Ash, ICAP 9000). The ICP-AES provided the quantitative chemical concentrations of measured elements (mg/L). The ICP-AES measurement limit is 10 $\mu g\ L^{-1}$ for Li and 5 $\mu g\ L^{-1}$ for Mn. The measured concentrations are typically more than 60 mg L^{-1} for Li, and 600 mg L^{-1} for Mn. The estimated error of the atomic ratios of Li/Mn is around 0.002, which is similar to the results in Ref. 15-17. The estimated errors can be one or two orders larger for samples with low concentrations, and a concentration of at least 20–80 mg L^{-1} is necessary to obtain a reasonable result. The ratios of oxygen and transition metals were determined qualitatively by relative peak areas of O/Kα and Mn/Lα, obtained from energy-dispersive X-ray spectroscopy (EDX).[15,16] The data was collected and corrected according to zero atomic force factors by a software package provided by Horiba, U.K. Film stresses were calculated from the curvatures of the substrates after deposition and annealing. The curvatures were measured by a laser interferometer.

The films deposited on stainless steel foils were packed in conventional coin cells with lithium foils as counter and reference electrodes. Charge–discharge and cyclic voltammetry tests were carried out using a μAutolab electrochemical measurement system (by Eco Chemie). The electrolyte was 1 M $LiPF_6$/ethyl carbonate-ethyl methyl carbonate (EC-EMC) (1:2) solution. All cells were charged under a constant voltage of 4.3 V vs Li/Li^+ until the current dropped bellow 1 μA, and discharged at a constant current density of 5 $\mu A\ cm^{-2}$.

Results and Discussion

Crystallography and composition.—Figure 1a shows the XRD patterns of the thin films deposited with various substrate biases. At 0 V_{dc} (i.e., no bias), the substrate was grounded. During deposition, the potential difference between the substrate and ground is less than 1 mV, which is therefore negligible compared with the negative bias applied. The ion-bombarding energy of the grounded sample is the difference between the plasma potential and ground. For the sample

* Electrochemical Society Student Member.
z E-mail: kfchiu@fcu.edu.tw

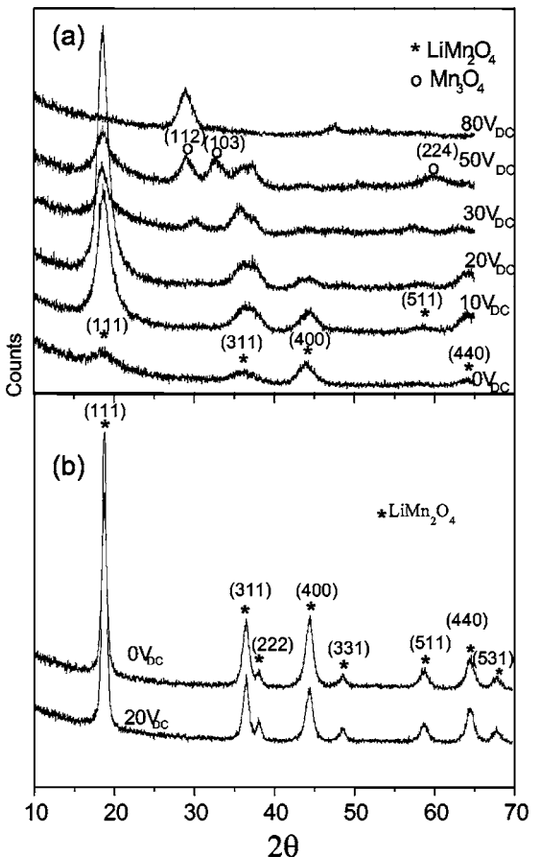

Figure 1. XRD patterns of (a) thin films deposited at different substrate bias and (b) 0 and 20 V_{dc} biased films after annealing in air at 600°C.

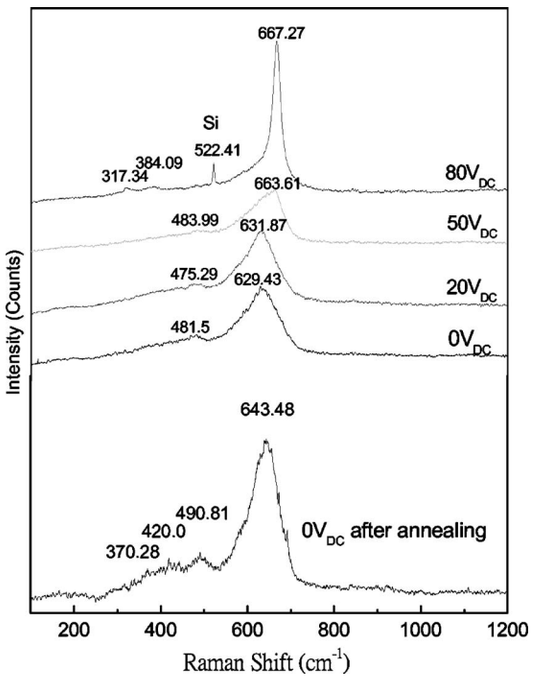

Figure 2. Raman spectra of thin films deposited at different substrate bias (0–80 V_{dc}) and the nonbiased film (0 V_{dc}) after annealing at 600°C in air.

at floating potential, the ion-bombarding energy is the different between the plasma and floating potential, which is therefore smaller than the grounded sample.

As shown in Fig. 1a, the 0 V_{dc} biased films exhibit poor crystallinity. Only a few broad peaks corresponding to spinel $LiMn_2O_4$ can be identified. The floating samples show poor crystallinity, similar to the grounded samples. As the applied bias increases (0–20 V_{dc}), a pronounced (111) peak develops. At too high a bias (>30 V_{dc}), the (111) peak starts to decrease, whereas a second phase develops and becomes predominant at higher bias. According to the ICCD-PDF database, the second phase may be Mn_3O_4. The films deposited at low bias (0 and 20 V_{dc}) were annealed in air at 600°C to increase the crystallinity. As shown in Fig. 1b, both films exhibit a well-crystallized $LiMn_2O_4$ spinel structure, and the diffraction patterns are nearly identical.

To further verify the structural evolution with different bias, micro-Raman spectra were measured as shown in Fig. 2. For bias of 0–30 V_{dc}, the films exhibit a broad band at wavenumber around 630 cm^{-1}, which is typical for defected or distorted spinel $Li_xMn_{2-y}O_4$.[17,18] At high bias (50–80 V_{dc}), this band shifts to higher wave number with stronger intensity. The results indicate that high bias not only enhances the film crystallinity, but also induces a structural transformation. The strong peak at 667 cm^{-1} (bias 80 V_{dc}) is the stretching mode (A_{1g}) of MnO_6 octahedra in a well-crystallized spinel structure, which can be attributed to the Mn_3O_4 spinel.[18] The Raman spectrum of well-crystallized $LiMn_2O_4$ spinel phase (0 V_{dc} after annealing) is also shown for comparison, where the A_{1g} mode is at wave number 643 cm^{-1}. Table I shows the ICP-AES and EDX results of the Li–Mn–O compositions for films deposited under different biases. Lithium content decreases due to high bias. The lithium content at 80 V_{dc} is bellow the detectable limit of ICP-AES, and the Mn/O ratio is 2.8/4, which is close to the stoichiometry of Mn_3O_4.

It can be concluded that suitable substrate bias can enhance the crystallinity of $LiMn_2O_4$ thin films and increase the relative intensity of (111) diffraction peaks. Too high a bias results in loss of Li and renders the structural transformation of $LiMn_2O_4$ toward a second phase. The loss of Li is due to resputtering caused by severe Ar-ion bombardment resulting from the negative substrate bias.

Surface morphology.—The surface morphologies of films deposited at different substrate biases are shown in Fig. 3. The substrate bias induces obvious morphology evolution. At 0 V_{dc} (Fig. 3a), the film is composed of nanosized primary grains (<10 nm) agglomerating into particles (~50 nm). As substrate bias increases, the spaces between the primary grains were reduced due to the enhanced adatom mobility by bias (Fig. 3b and c). The agglomerates also become larger (~100 nm). At high bias (80 V_{dc}) the film morphology is smooth with a few particles dispersed nonuniformly on the surface, as shown in Fig. 3d. The composition of these particles is still unknown. They might be amorphous lithium oxides, which are not detectable in XRD and EDX measurements.

Figure 4a and b shows the surface morphology of the air-annealed (600°C) films deposited with substrate bias of 0 and

Table I. Chemical compositions of $Li_xMn_{2-y}O_4$ thin films deposited at different substrate biases.

	Li	Mn	O
Powder from target (V_{dc})	1.29	2	~4
0	1.34	2	~4
−10	1.33	2	~4
−20	1.32	2	~4
−30	1.30	2	~4
−50	0.98	2	~4
−80	-	2.8	~4

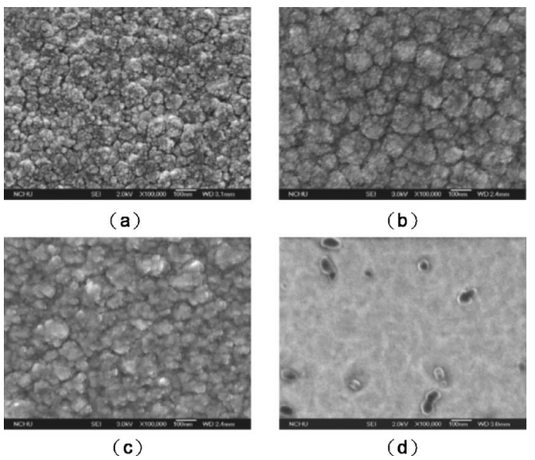

Figure 3. Surface morphologies of thin films deposited at substrate bias (a) 0, (b) 20, (c) 30, and (d) 80 V_{dc}.

20 V_{dc}, respectively. After annealing, the film of bias 0 V_{dc} exhibits obvious necking between the agglomerates with loose spaces among them, and the original nanosized primary grains can still be observed. For the film deposited with bias of 20 V_{dc}, the annealed film shows a dense morphology with flake-like large grains. These surface morphologies are completely different (Fig. 4a and b), and interestingly, the XRD patterns of these films are nearly identical (Fig. 1b). This provides a good example for studying the influences of surface morphology on electrochemical performance.

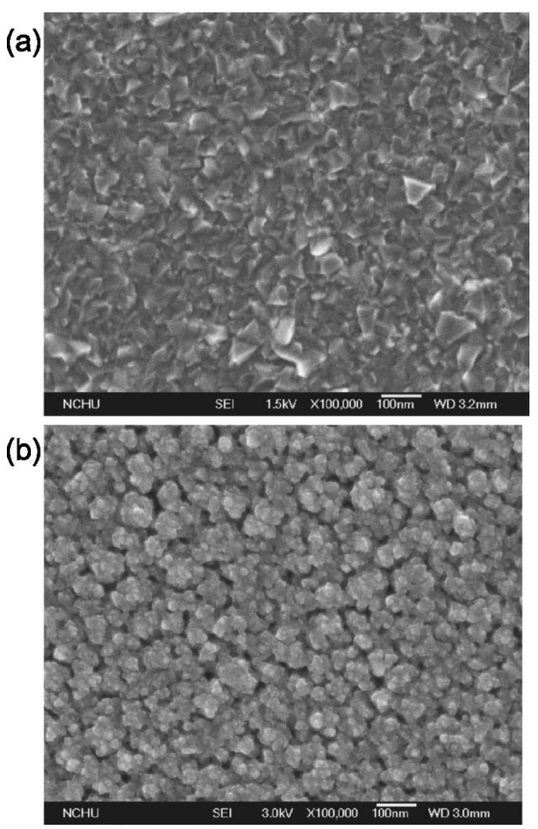

Figure 4. Surface morphologies of (a) 0 V_{dc} and (b) 20 V_{dc} biased films after annealing at 600°C in air.

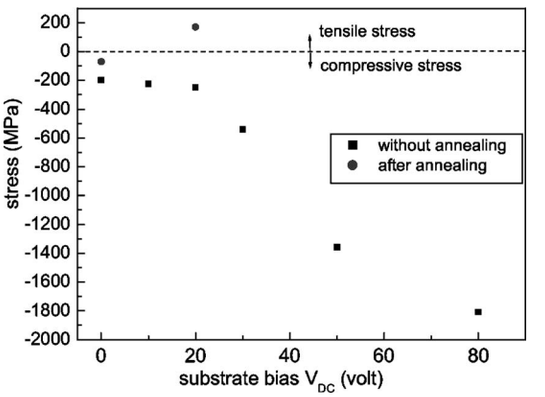

Figure 5. Film stress as a function of substrate bias. The stress of films after postannealing at 600°C in air is indicated by circles.

Film stress.—Figure 5 shows the film stress as a function of substrate bias. It is well-known that thin films deposited under concurrent ion bombardment can develop compressive stress. The substrate bias accelerates the ions to bombard the film surface and push the adatoms into spaces smaller than the atomic volumes, resulting in compressive stress.[19,20] However, the dramatic increase of compressive stress (for bias >30 V) cannot be attributed to the ion bombardment alone. Development of the second phase (such as Mn_3O_4) may be responsible for the sudden increases of compressive stress for bias over 30 V_{dc}.

For the films deposited at 0 and 20 V_{dc} bias, the compressive stress relaxes after annealing as shown in Fig. 5. The stress of 20 V_{dc} biased film becomes tensile after annealing. It is due to the formation of a much denser film after annealing, which results in the shrinkage of film volume and therefore induces a tensile stress in order to maintain the stress equilibrium in the film/substrate system.

Electrochemical tests.—Figure 6 shows the initial discharge characteristics for the films modified under different process parameters. Because a certain amount of defected and distorted crystallites in the sputtered films is almost inevitable, as a result all films have capacities less than the theoretical value at a cutoff voltage of 3.0 V. The 0 V_{dc} biased films show low discharge voltage. Substrate bias as low as 10 V_{dc} can effectively elevate the discharge voltage and capacity. The 20 V_{dc} biased films show the best results among the unannealed samples due to the relatively higher crystallinity and pure phase. The discharge curve (20 V_{dc}) exhibits a sloppy plateau, gradually decreasing from 4.4 to 3.8 V, but shows a capacity as high as 121 mAh/g. Higher bias (i.e., 30 V_{dc}) results in slightly lower

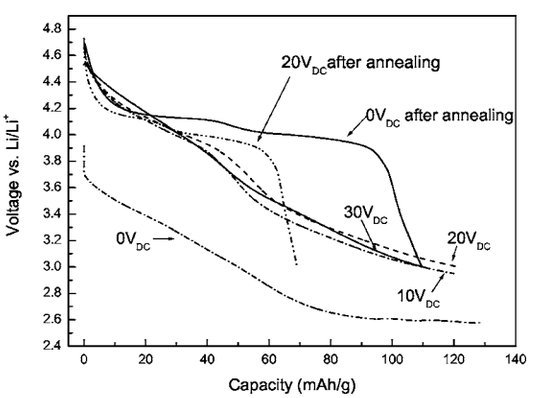

Figure 6. Initial discharge curves for films prepared with different process parameters.

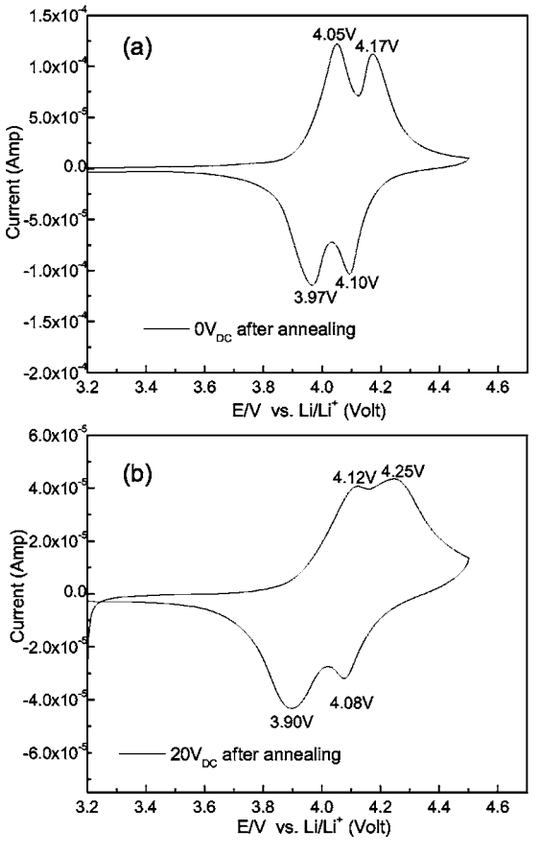

Figure 7. CV curves of (a) 0 and (b) 20 V_{dc} biased films after annealing at 600°C in air.

capacity and a more sloppy discharge curve, which may be due to the development of the second phase (Fig. 1a). For the postannealed thin films, the discharge curves show the typical 4.1 and 3.9 V plateaus of the $LiMn_2O_4$ cathodes, which indicates that well-crystallized $LiMn_2O_4$ phase is essential for high discharge voltage. The film treated with 0 V_{dc} bias and postannealing exhibits a much larger discharge capacity than the film with 20 V_{dc} bias and postannealing. The surface morphology might be responsible for the difference in the discharge capacity. As shown in Fig. 4a and b, the much dense morphology for the 20 V_{dc} biased films after annealing may have smaller effective surface for reaction, compared with the loose morphology of 0 V_{dc} biased films after annealing.

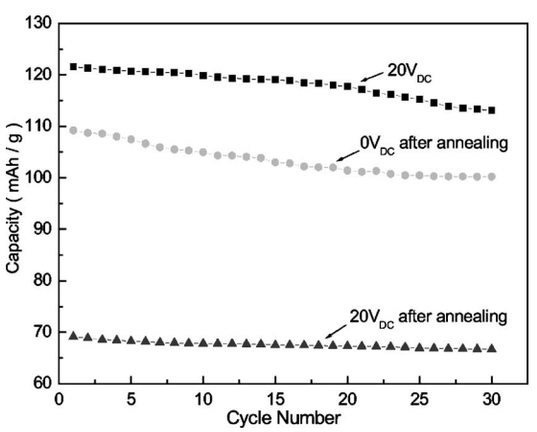

Figure 8. Discharge capacities as a function of cycle number.

Table II. Discharge capacity (mAh/g) at different cycles. The capacity loss compared with the initial cycle is shown in the parenthesis.

	Cycle 1	Cycle 10	Cycle 20	Cycle 30
−20 V dc	121.56	119.88(1.4%)	117.75(3.2%)	113.10(6.9%)
0 V dc + anneal	109.19	104.95(3.8%)	101.39(7.1%)	100.19(8.3%)
−20 V dc + anneal	69.13	67.80(1.9%)	67.31(2.6%)	66.70(3.5%)

The influence of surface morphology on the redox processes is shown in the cyclic voltammetry (CV) curves (Fig. 7a and b) with a sweep rate of 0.16 mV/s. The 0 V_{dc} biased and annealed films (Fig. 7a) exhibit well-resolved redox peaks compared with 20 V_{dc} biased and annealed ones, indicating that the large agglomerates composed of small grains (Fig. 4a) may favor the lithium-ion intercalation/deintercalation process, whereas larger grains and dense surfaces (Fig. 4b) do not.

Another possible cause of the capacity difference between the 0 and 20 V_{dc} biased films after annealing is the large stress variation (Fig. 5). As the stress varies from compression to tension, some parts of the film may break or peel off, which then become inactive due to loss of electric contact with the current collector. As a result, the 20 V_{dc} biased and annealed films show lower capacity. To distinguish the effects of surface morphology and stress, lithium transport rates may be necessary and will be investigated in the immediate future.

Figure 8 shows the discharge capacity as a function of cycle number up to 30 cycles. All selected films show good reversible properties. The capacities and the percentages of capacity loss at different cycles are summarized in Table II. It is interesting that the 20 V_{dc} biased films exhibit relatively better capacity retention whether before or after annealing. It may indicate that the substrate bias during film growth can increase the material integrity and reduce capacity fading. For 20 V_{dc} biased films after annealing, the capacity loss is only 3.5% after 30 cycles, despite the lower reversible capacity recorded.

For vacuum deposition processes the parameters might vary from chamber to chamber due to different geometric configurations and target properties, such as size, process-history, and mounting quality. Especially for different chamber and target sizes, the effective bias values may be different, because the plasma potential changes accordingly. The work demonstrated here was carried out on a well-mounted 2-in. pure target. A total sputtering time of approximately 200 h was used. During this period, the sample quality was frequently checked based on crystallinity and resistivity and showed high reproducibility.

Conclusion

Thin films of $Li_xMn_{2-y}O_4$ have been prepared by bias rf sputter deposition. It has been demonstrated that the substrate bias can increase the relative intensity of the (111) diffraction peak and modify the surface morphology of the films. High bias may result in loss of Li content and formation of manganese oxide second phase. An initial discharge capacity as high as 121 mAh/g can be achieved by applying 20 V_{dc} bias during film growth. The films postannealed at 600°C in air exhibit high (4.1–3.9 V) and flat voltage plateaus, which indicate that well-crystallized $LiMn_2O_4$ spinel phase is essential for achieving high-discharge voltage plateaus. After annealing, the 20 V_{dc} biased films show much lower discharge capacity, which may be attributed to the dense morphology and the large stress variation. By applying well-tuned substrate bias and annealing, the $Li_xMn_{2-y}O_4$ thin-film properties can be modified. The biased samples have higher discharge capacity and voltage compared with nonbiased samples. The 20-V_{dc} sample exhibits higher capacity than the annealed samples with a slightly lower capacity

loss rate. However, discharge voltage near 4.0 V can only be obtained by postanneal. The capacity loss as low as 3.5% after 30 cycles can be achieved by applying 20 V_{dc} bias and postanneal with the expense of lower capacity.

Acknowledgments

The authors thank Dr. H. L. Liu for Raman spectrum measurements. This research was sponsored by R.O.C. National Science Council under contract no. NSC 93-2216-E-035-024, and by Feng Chia University under contract no. FCU92-GB-12.

Feng Chia University assisted in meeting the publication costs of this article.

References

1. B. Wang, J. B. Bates, F. X. Hart, B. C. Sales, R. A. Zuhr, and J. D. Robertson, *J. Electrochem. Soc.*, **143**, 3203 (1996).
2. J. B. Bates, N. J. Dudney, B. J. Neudecker, F. X. Hart, H. P. Jun, and S. A. Hackney, *J. Electrochem. Soc.*, **147**, 59 (2000).
3. S. Nieto-Ramos, M. S. Tomar, S. Hernandez, and F. Aliev, *Thin Solid Films*, **337-338**, 745 (2000).
4. J. B. Bates, N. J. Dudney, D. C. Lubben, G. R. Gruzalski, B. S. Kwak, X. Yu, and R. A. Zuhr, *J. Power Sources*, **54**, 58 (1995).
5. J. B. Bates, N. J. Dudney, G. R. Gruzalski, R. A. Zuhr, A. Choudhury, C. F. Luck, and J. D. Robertson, *J. Power Sources*, **43-44**, 103 (1993).
6. B. Wang, B. S. Kwak, B. C. Sales, and J. B. Bates, *J. Non-Cryst. Solids*, **183**, 297 (1995).
7. S. D. Jones and J. R. Akridge, *J. Power Sources*, **54**, 63 (1995).
8. K. H. Hwang, S. H. Lee, and S. K. Joo, *J. Electrochem. Soc.*, **141**, 3296 (1994).
9. R. Goldner, T. Y. Liu, S. Slaven, A. Gerouki, P. Zerigian, T. E. Haas, F. O. Arntz, and S. Jones, in *Thin Film Solid Ionic Devices and Materials*, J. B. Bates, Editor, PV 95-92, p. 173, The Electrochemical Society Proceedings Series, Pennington, NJ (1996).
10. Y. J. Park, J. G. Kim, M. K. Kim, H. T. Chung, W. S. Um, M. H. Kim, and H. G. Kim, *J. Power Sources*, **76**, 41 (1998).
11. Y. J. Park, K. S. Park, J. G. Kim, M. K. Kim, H. G. Kim, and H. T. Chung, *J. Power Sources*, **88**, 250 (2000).
12. C. Julien, E. Haro-Poniatowski, M. A. Camacho-Lopez, L. Escobar-Alarcon, and J. Jimenez-Jarquin, *Mater. Sci. Eng., B*, **72**, 36 (2000).
13. K. Ozawa, *Solid State Ionics*, **69**, 212 (1994).
14. M. Wakihara and O. Yamamoto, *Lithium Ion Batteries*, p. 15, Kodansha and Wiley-VCH, Tokyo (1998).
15. N. J. Dudney, J. B. Bates, R. A. Zuhr, S. Young, J. D. Robertson, H. P. Jun, and S. A. Hackney, *J. Electrochem. Soc.*, **146**, 2455 (1999).
16. K.-F. Chiu, F. C. Hsu, G. S. Chen, and M. K. Wu, *J. Electrochem. Soc.*, **150**, 503 (2003).
17. K.-F. Chiu, H. H. Hsiao, G. S. Chen, H. L. Liu, J. L. Her, and H. C. Lin, *J. Electrochem. Soc.*, **151**, 452 (2004).
18. C. M. Julien and M. Massot, *Mater. Sci. Eng., B*, **97**, 217 (2003).
19. R. D. Bland, G. J. Kominiak, and D. M. Mattox, *J. Vac. Sci. Technol.*, **11**, 671 (1974).
20. M. Wakihara, G. Li, and H. Ikuta, in *Lithium Ion Batteries, Fundamentals and Performance*, M. Wakihara and O. Yamamoto, Editors, p. 35, Kodansha, Ltd., Tokyo, Japan (1998).